ARTICLE IN PRESS

Available online at www.sciencedirect.com
ScienceDirect
Journal of Photochemistry and Photobiology B: Biology 90 (2008) 187–197
Journal of Photochemistry and Photobiology B:Biology
www.elsevier.com/locate/jphotobiol

Resonance energy transfer and ligand binding studies on pH-induced folded states of human serum albumin

Ajay Kumar Shaw, Samir Kumar Pal *

Unit for Nano Science and Technology, Department of Chemical, Biological and Macromolecular Sciences, S.N. Bose National Centre for Basic Sciences, Block JD, Sector III, Salt Lake, Kolkata 700 098, India

Received 21 August 2007; received in revised form 2 January 2008; accepted 2 January 2008

Abstract

Human serum albumin (HSA) is a very important transporter protein in the circulatory system. It is a multi-domain binding protein, which binds a wide variety of ligands in its multiple binding sites and aids in transport, distribution and metabolism of many endogenous and exogenous ligands. With change in pH, HSA is known to undergo conformational transformation, which is very essential for picking up and releasing them at sites of differing pH inside physiological system. Hence, the characterization of ligand binding to these pH-induced conformers is extremely important. We have explored binding interaction of a ligand protoporphyrin IX (PPIX), which is demonstrated (X-ray crystallography) to reside in domain-IB at the various pH-induced folded states of HSA. The ligand PPIX is found to remain attached to all the HSA conformers which offers an opportunity to use Förster's resonance energy transfer (FRET) between an intrinsic donor fluorophore (Trp214) located in domain-IIA to the acceptor ligand PPIX to characterize the inter-domain separation between IB and IIA. Additionally FRET between an extrinsic fluorophore 2-*p*-toluidinylnaphthalene-6-sulfonate (TNS) located in domain-IIIA and PPIX is also undertaken to quantify the inter-domain separation between IB and IIIA. Circular dichroism (CD) and dynamic light scattering (DLS) studies have been done in conjunction with picosecond time resolved fluorescence and polarization-gated spectroscopy to determine, respectively, the secondary and tertiary structures of various pH-induced folded states of the protein. Severe structural perturbation including swelling of the protein is observed in the low pH-induced conformer of HSA as evidenced from all the techniques used.

Keywords: Human serum albumin (HSA); FRET; Fluorescence anisotropy; PPIX–HSA complex; Inter-domain separation

1. Introduction

Serum albumins are multi-domain proteins forming the major soluble protein constituent of the circulatory system [1]. These are engaged with various physiological functions involving maintenance of osmotic blood pressure, transportation of a wide variety of ligands in and out of the physiological system. Human serum albumin (HSA) (molecular weight 66,479 Da) is a heart-shaped tridomain protein with each domain comprising of two identical subdomains A and B [2] (see Scheme 1). HSA having 585 amino acid residues assumes solid equilateral triangular shape with sides ~80 Å and depth ~30 Å [3]. Its amino acid sequence comprises of 17 disulfide bridges distributed over all domains, one free thiol (Cys34) in domain-I and a tryptophan residue (Trp214) in domain-IIA. The protein binds various kinds of ligands [4] including photosensitizing drugs [5] and the principal binding regions are located in subdomains-IIA and -IIIA of which IIIA binding cavity is the most active one [3]. Porphyrins are a class of tetrapyrroles that have extensive applications as photosensitizing drugs in medicine [6,7]. Serum albumins and low and high density lipoproteins acts as the endogenous carriers of porphyrins in circulation [8,9]. The photophysics of porphyrins are very well studied [10–17]. Porphyrins are known to form aggregates and they serve as models for

* Corresponding author. Fax: +91 33 2335 3477.
E-mail address: skpal@bose.res.in (S.K. Pal).

1011-1344/$ - see front matter © 2008 Elsevier B.V. All rights reserved.
doi:10.1016/j.jphotobiol.2008.01.001

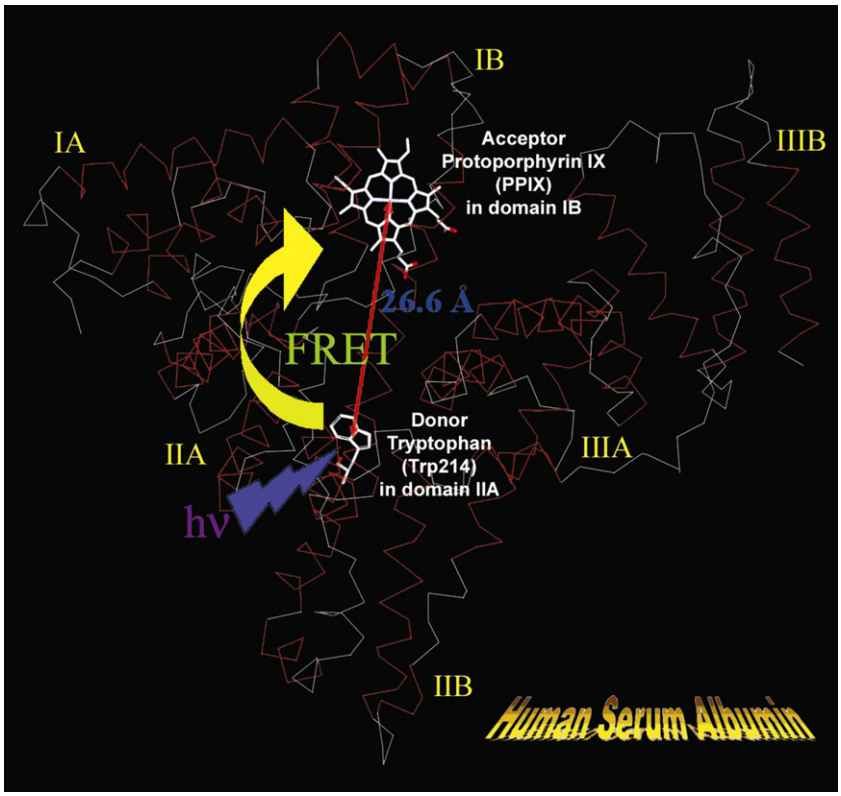

Scheme 1. X-ray crystal structure of human serum albumin depicting the FRET between the donor tryptophan (Trp214) and the acceptor Protoporphyrin IX (PPIX). Different subdomains are marked in yellow. (For interpretation of the references to color in this figure legend, the reader is referred to the web version of this article.)

artificial solar energy capture as in photosynthesis [18]. Basically the aggregates are of two types – J-aggregates, where molecular rearrangement is end-to-end with red shift of absorption and H-aggregates, where the rearrangement is face-to-face with blue shift of absorption band as predicted by Exciton theory [19]. The thermodynamics and kinetics of porphyrin aggregation are well documented in literature [12,20]. The interaction of porphyrins with serum albumins has also been a subject of extensive research till date [21–25]. Protoporphyrin IX (PPIX), a member of porphyrin family, was shown to bind to domain-IB of HSA, as evident from the X-ray crystallographic study [5].

Studies on binding of various drugs/ligands to HSA at its different folded states are important as the conformation of the carrier protein depends on its immediate physiological environment. Also, recent advancement in the field of nanosciences requires the preparation of bioactive nanoparticles under different temperature and pH conditions using protein molecules as templates [26–28]. Hence, search for a protein molecule, which can retain its overall structure under conditions widely differing from the physiological condition is highly demanding. It is known that HSA undergoes reversible conformational transformation with change in pH of the solution containing the protein [29,30]. At normal pH 7, HSA assumes the normal form (N) which abruptly changes to fast migrating form at pH values less than 4.3. Upon further reduction in pH to less than 2.7 the F-form changes to the fully extended form (E). On the basic side of the normal pH above pH 8, the N-form changes to basic form (B) and above pH 10, the structure changes to another aged form (A) [31]. By using picosecond time-resolved polarization gated spectroscopy, we have explored the nature of binding of PPIX in various pH-induced conformers of HSA. The interactions of PPIX in domain-IB in the different conformers of the protein and significant spectral overlap of PPIX-absorption with that of the emission of Trp214 (domain-IIA) offer opportunity to measure inter-domain distance in various conformations of HSA by using picosecond resolved Förster's resonance energy transfer (FRET). We have also explored another inter-domain distance between PPIX (domain-IB) and an extrinsic fluorophore 2-*p*-toluidinylnaphthalene-6-sulfonate (TNS) (domain-IIIA). Dynamic light scattering (DLS) and Circular dichroism (CD) have been used to further characterize the pH-induced folded states.

2. Materials and methods

Human serum albumin (HSA), protoporphyrin IX (PPIX), 2-*p*-toluidinylnaphthalene-6-sulfonate (TNS), sodium acetate, sodium dihydrogen phosphate, disodium hydrogen phosphate were procured from sigma chemical (St. Louis, USA). Hydrochloric acid, sodium hydroxide and dimethyl formamide (DMF) were procured from Merck. Double distilled water was used for preparation of aqueous solutions. The molecular weight of HSA has

been checked by MALDI mass spectrometry which essentially reveals a peak at 66.8 kDa (data not shown) consistent with the literature value [2]. All the other samples were used as received without further purification. Alkaline pH solutions were prepared by adding NaOH to phosphate buffer, while acidic pH solutions were prepared by adding HCl to acetate buffer. A Stock solution of HSA was prepared in 10 mM phosphate buffer solution. HSA was labeled with PPIX as follows. About 3.5 mg of PPIX was dissolved in 100 μl DMF and injected in five aliquots of 20 μl each to 2 ml of phosphate buffer containing 200 μM HSA at an interval of 15 min under vigorous stirring condition. The mixture is allowed to vigorously stir for 1 h and then a mild dialysis was carried out against phosphate buffer for 4.5 h to remove the unreacted PPIX. The HSA–PPIX complex is formed in the ratio 1:1, which ensures better energy transfer. The HSA–PPIX solution was added in equal amounts to measured volumes of acidic/alkaline pH solutions and allowed to stir vigorously for 2 h in order to achieve various pH-induced conformers of HSA–PPIX complexes. In order to label HSA and HSA–PPIX complex with TNS, calculated volume of concentrated TNS solution was added to a definite volume of HSA solution so that the concentration ratio of TNS:HSA remains 1:1 and the mixture was then stirred vigorously for an hour. Complexes of TNS with HSA and HSA–PPIX were then used for various steady-state and time-resolved experiments.

Steady-state absorption and emission were measured with Shimadzu UV-2450 spectrophotometer and Jobin Yvon Fluoromax-3 fluorimeter, respectively. The circular dichroism study was done using Jasco 815 spectropolarimeter using a quartz cell of path-length 10 mm. The secondary structural data of the CD spectra were analyzed using CDNN deconvolution program. Dynamic light scattering (DLS) measurements were done with Nano-S Malvern instruments (UK), employing a 4 mW He–Ne laser ($\lambda = 632.8$ nm) and equipped with a thermostatted sample chamber. All measurements were taken at 173° scattering angle at 298 K. The scattering intensity data are processed using the instrumental software to obtain the hydrodynamic diameter (d_H) and the size distribution of the scatterer in each sample. The instrument measures the time dependent fluctuation in intensity of light scattered from the particles in solution at a fixed scattering angle. Hydrodynamic diameters (d_H) of the particles are estimated from the intensity autocorrelation function of the time-dependent fluctuation in intensity. d_H is defined as, $d_H = k_B T/3\pi\eta D$, where k_B is the Boltzmann constant; T, the absolute temperature; η, the viscosity and D, the translational diffusion coefficient. In a typical size distribution graph from the DLS measurement X-axis shows a distribution of size classes in nm, while the Y-axis shows the relative intensity of the scattered light. This is therefore known as an intensity distribution graph.

All the fluorescence transients were recorded using picosecond-resolved time correlated single photon counting (TCSPC) technique at 54.7° (magic angle) with respect to polarization axis of the excitation beam. The TCSPC setup was from Edinburgh instruments (LifeSpec-ps), UK. In order to excite TNS and PPIX excitation laser sources of wavelengths 375 nm [instrument response function (IRF) ~ 76 ps] and 409 nm (IRF ~ 86 ps), respectively, were used. Excitation of the tryptophan residue of HSA was made by a LED source of wavelength 299 nm (IRF ~ 460 ps). The observed fluorescence transients are fitted by using a nonlinear least square fitting procedure [32] (software supplied by Edinburgh Instruments) to a function,

$$X(t) = \int_0^t E(t')R(t-t')\mathrm{d}t' \tag{1}$$

comprising of convolution of the IRF ($E(t)$) with a sum of exponentials,

$$R(t) = A + \sum_{i=1}^{N} B_i \mathrm{e}^{t/\tau_i} \tag{2}$$

with pre-exponential factors (B_i), characteristic lifetimes (τ_i) and a background (A). Relative concentration of a characteristic lifetime in a multi-exponential decay is finally expressed as

$$\alpha_n = \frac{B_n}{\sum_{i=1}^{N} B_i} \times 100 \tag{3}$$

The average lifetime (amplitude-weighted) of decay [33] was expressed as

$$\langle\tau\rangle = \sum_{i=1}^{N} \alpha_i \tau_i. \tag{4}$$

The quality of the curve fitting was evaluated by reduced chi-square (0.90–1.1) and residual data. The purpose of the fitting is to obtain the decays in an analytic form suitable for further data analysis. For the temporal fluorescence anisotropy, $r(t)$ measurements emission polarization was adjusted to be parallel or perpendicular to that of the excitation and defined anisotropy as

$$r(t) = \frac{I_{II}(\mathrm{t}) - GI_{\perp}(\mathrm{t})}{I_{II}(\mathrm{t}) + 2GI_{\perp}(\mathrm{t})} \tag{5}$$

The G-factor at a given wavelength was independently obtained by exciting the sample with a horizontally polarized excitation beam and collecting the two polarized fluorescence decays, one parallel and other parallel to the horizontally polarized excitation beam [34]. The $r(t)$ was analyzed using sum and difference analysis of the time resolved polarized intensities and fitted to a multi-exponential function using the expression $r(t) = r_\infty + \sum_i \beta_i \mathrm{e}^{-t/\varphi_i}$, where φ_i is the rotational time constant; r_∞, the limiting anisotropy; β_i, their amplitudes; and initial anisotropy, $r_0 = r_\infty + \sum \beta_i$. We have considered a non-associative model and have not linked a particular fluorescence lifetime to a particular rotational time constant. In order to find out the semicone angle inscribed by a wobbling dye molecule bound to a rigid macrmolecule, we assume $\sum \beta_i = 1$ and the β_2 value corresponding to longer rotational time constant (φ_2, for

biexponential decay) equals to the square of order parameter S [35,36] and is defined as

$$\beta_2 = S^2 = \left[\frac{1}{2}\cos\theta_w(1+\cos\theta_w)\right]^2 \quad (6)$$

In order to estimate the fluorescence resonance energy transfer efficiency of the donor Trp214 and TNS and hence to determine distances of donor–acceptor pairs, we followed the methodology described in chapter 13 of Ref. [33]. The Förster distance (R_0) is given by

$$R_0 = 0.211[\kappa^2 n^{-4} Q_D J(\lambda)]^{1/6} \text{ (in Å)}, \quad (7)$$

where κ^2 is a factor describing the relative orientation in space of the emission and absorption transition dipoles of the donor and acceptor, respectively. The value of the orientation factor κ^2 is calculated from the equation [33],

$$\kappa^2 = (\sin\theta_D \sin\theta_A \cos\phi - 2\cos\theta_D \cos\theta_A)^2, \quad (8)$$

where φ is the dihedral angle between the planes containing emission transition dipole of the donor and absorption transition dipole of the acceptor and θ_D and θ_A are the angles between these dipoles and the vector joining the donor and acceptor [37]. The refractive index (n) of the medium is assumed to be 1.4. Q_D, the quantum yield of the donor in the absence of acceptor is measured using the quantum yield of pure tryptophan (0.14) in buffer (pH 7) for Trp214 of HSA and that of C500 (0.76) in *n*-hexane [38] for TNS bound to HSA at different pH(s). $J(\lambda)$, the overlap integral, which expresses the degree of spectral overlap between the donor emission and the acceptor absorption is given by

$$J(\lambda) = \frac{\int_0^\infty F_D(\lambda)\varepsilon_A(\lambda)\lambda^4 d\lambda}{\int_0^\infty F_D(\lambda)d\lambda}, \quad (9)$$

where $F_D(\lambda)$ is the fluorescence intensity of the donor in the wavelength range of λ to $\lambda + d\lambda$ and is dimensionless. $\varepsilon_A(\lambda)$ is the extinction coefficient (in $M^{-1}\,cm^{-1}$) of the acceptor at λ. If λ is in nm, then $J(\lambda)$ is in units of $M^{-1}\,cm^{-1}\,nm^4$. Once the value of R_0 is known, the donor–acceptor distance (R) can easily be calculated using the formula,

$$R^6 = [R_0^6(1-E)]/E \quad (10)$$

Here, E is the efficiency of energy transfer. The transfer efficiency is measured using the average lifetimes of the donor in the absence, $\langle\tau_D\rangle$ and presence of acceptor, $\langle\tau_{DA}\rangle$ as follows:

$$E = 1 - (\langle\tau_{DA}\rangle/\langle\tau_D\rangle) \quad (11)$$

The donor–acceptor distances (R) are measured using the above equations. The concentration of protein used for fluorescence measurement was about 7 μM in order to avoid intermolecular energy transfer between two protein molecules.

3. Results and discussion

Fig. 1a shows the size distribution graph of various conformations of HSA in buffer solutions of different pH obtained through dynamic light scattering studies. The

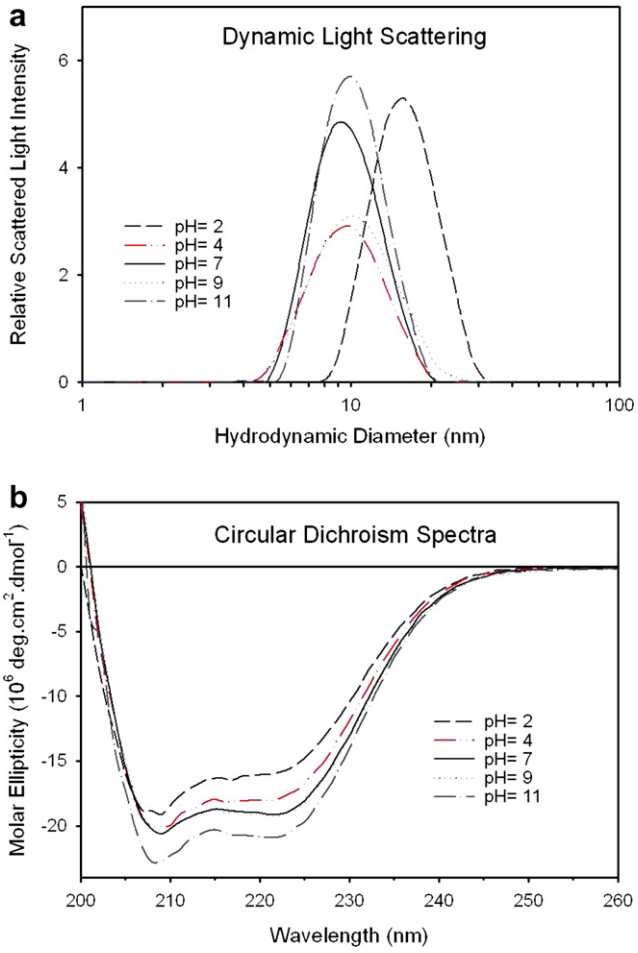

Fig. 1. (a) Dynamic light scattering spectra (DLS) and (b) Circular Dichroism (CD) spectra of HSA in buffer solutions of various pHs.

hydrodynamic diameters of different conformations are as follows: 16.4 nm (E-form, pH 2), 10.2 nm (F-form, pH 4), 10.4 nm (N-form, pH 7), 10.7 nm (B-form, pH 9) and 10.4 nm (A-form, pH 11). The above hydrodynamic data indicate that in the acidic pH buffer solutions the globular structure adopted by HSA in normal pH solution undergo swelling with a significant change in tertiary structure. However, in the basic pH buffer solution such structural stretching is not observed. Application of Stokes–Einsein–Debye (SED) relation [39], $\tau_{rot} = \frac{4\pi\eta r_H^3}{3k_B T}$ on the hydrodynamic radius r_H obtained from DLS gives the following overall rotational time (τ_{rot}) constants of different pH-induced conformers of HSA: E-form, 507 ns; F-form, 122 ns; N-form, 129 ns; B-form, 141 ns; A-form, 129 ns. η, k_B and T represent the dispersant viscosity, Boltzmann constant and temperature in Kelvin scale. From the CD studies (Fig. 1b and Table 1) it is observed that in addition to the disruption of tertiary structure (DLS studies) there is a significant loss in helicity when HSA changes its conformation from N-form to E-form. The observation is consistent with another study [40] which confirms a significant loss in helical content with a structural loosening at the C-terminal end followed by separation of domains and

Table 1
Percentages of secondary structures in different conformations of Human serum albumin (HSA) at different pH(s)

Secondary structures	HSA in buffer solutions of different pH(s)				
	2	4	7	9	11
Helix (%)	59.00	64.70	67.10	67.10	60.40
Antiparallel (%)	4.00	3.40	3.20	3.20	3.90
Parallel (%)	4.10	3.50	3.20	3.20	4.00
Turns (%)	13.20	12.50	12.20	12.20	13.00
Random (%)	19.70	15.90	14.30	14.30	18.70

subdomains in the N–F transition during acid-induced unfolding of HSA. Further reduction of pH below 3.5 when HSA assumes E-form at pH 2, the domain-I undergoes expansion leading to the disruption of intra-domain structure in this pH region. Domain-II is, however, known to assume molten globule state in N–F transition [40]. In the alkaline pH range, during N–B transition, contrary to the previous study [40], there is no change in helicity content. However, at pH 11 the A-conformer shows a decrease in the helicity content compared to the native form of HSA (N-form) at normal pH.

Fig. 2a shows the fluorescence spectra (excitation wavelength = 297 nm) of various conformations of HSA at three different pH(s). The fluorescence is solely due to the excitation of Trp214 residue of HSA located in the binding domain-IIA at the bottom of a 12 Å deep crevice [31]. The N-form has a fluorescence maximum at 337 nm consistent with previous studies [31,40]. The E-form has a fluorescence maximum at 332 nm while for the A-form it is at 335 nm, both of which are blue shifted compared to the N-form. These changes are consistent with previous studies [31,40] indicating that although at pH 2 the inter-domain separation increases with the disruption of deep crevice, the rearrangement of the local environment around Trp214 causes it to be in more hydrophobic environment of the protein matrix [41]. At alkaline pH 11, that is in A-form, Trp214 is present in slight hydrophobic environment due to minor changes in secondary structure. Fig. 2b shows the absorption and emission spectra (excitation wavelength = 409 nm) of PPIX labeled HSA at different pH(s). Porphyrins form a class of molecules whose physicochemical properties depends on the state of ionization of the molecules [42] and the ionization is associated with the acid–base properties of both the imino and pyrrole nitrogens of the ring structures and the peripheral groups attached to the molecule [43]. The conjugated ring structure of porphyrin is responsible for the spectral feature of this drug molecule; as a result the protonation of imino nitrogen should influence the electron distribution of the chromophore and thus the spectral properties. The N-form HSA has an absorption maximum at 412 nm corresponding to the Soret band while the other peaks between 500 nm and 700 nm are the Q-bands [10,44,45]. At acidic pH for E-form HSA, the intensity of Soret band decreases and the absorption maximum exhibits a blue shift to 386 nm. At alkaline pH 11, the absorption spectrum is similar to that at pH 7 with a lower intensity of the soret band. The emission spectra of PPIX labeled HSA at pH 7 and 11 have an intense emission peak at 633 nm. However, at pH 2, this band at 633 nm decreases in intensity with the appearance of two new peaks at 600 nm and 658 nm. These new peaks may arise due to the protonation of imino nitrogens in the porphyrin ring [43]. The variation in the spectra of PPIX with pH indicates that the probe with the protein at various conformations is efficient in sensing the immediate environment of HSA.

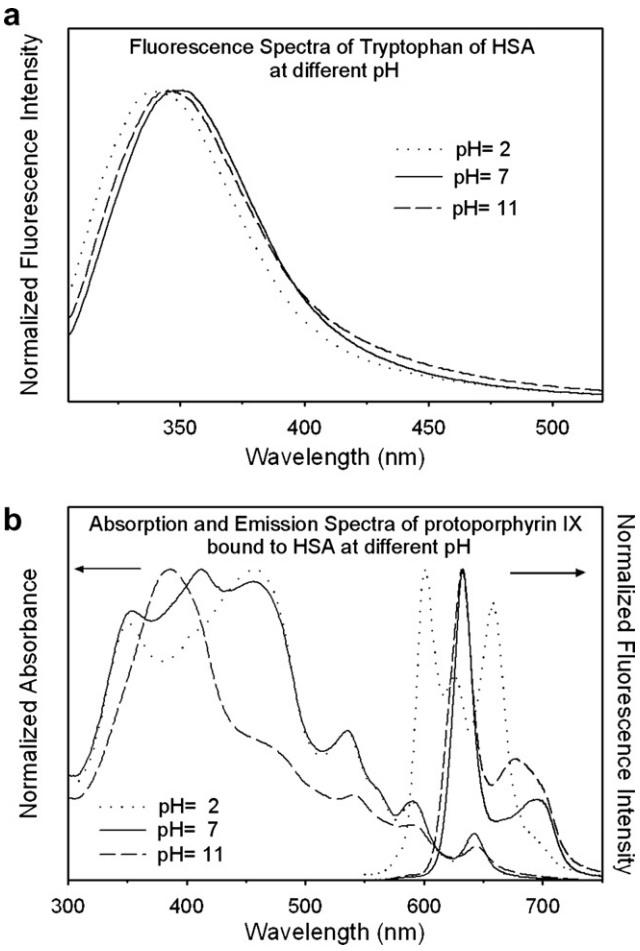

Fig. 2. (a) Fluorescence spectra of Tryptophan (Trp214) residue of HSA (excitation = 297 nm) and (b) absorption and fluorescence spectra of protoporphyrin IX (PPIX) bound to HSA (excitation = 409 nm) at three pH(s).

Fig. 3a shows the fluorescence transients of PPIX bound to HSA at pH 2, 7 and 11 at 632 nm (excitation wavelength = 409 nm). Table 2 depicts the fluorescence lifetime of PPIX bound to HSA at five different pH(s), which are essentially non-exponential in nature [46]. In all the cases, three time components in the range of 0.2–0.4 ns, 2–4 ns and 9–14 ns are observed. The time constants are in fair agreement with a previous study [46] except the shortest one whose contribution towards fluorescence is very small (<1%) and might have been neglected in the earlier study. Fig. 3b–d depicts the temporal fluorescence anisotropy decay curve of PPIX–bound HSA at pH 2, 7 and 11. At

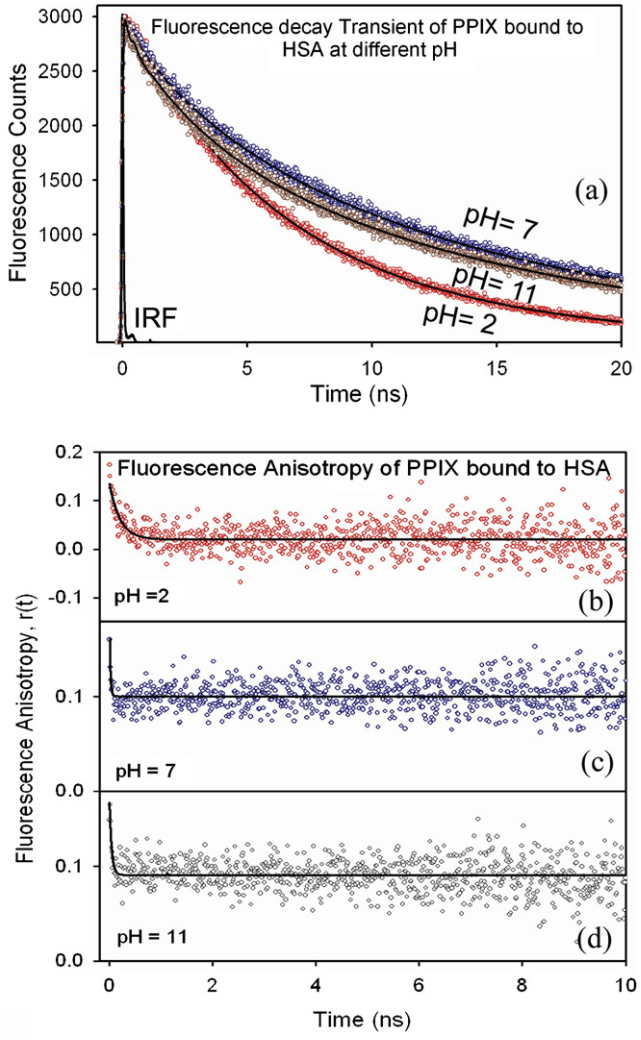

Fig. 3. (a) Fluorescence decay transients and temporal fluorescence anisotropy decay of PPIX bound to HSA (emission = 632 nm) at pH(s) (b) 2, (c) 7 and (d) 11.

Table 2
Fluorescence lifetimes (τ) of protoporphyrin IX bound to HSA at different pH(s)

Samples	τ_1 (ns)	τ_2 (ns)	τ_3 (ns)
PPIX (pH 2)	0.19 (14.3)	4.77 (40.7)	8.97 (45.0)
PPIX (pH 4)	0.34 (15.6)	3.40 (17.8)	14.55 (66.7)
PPIX (pH 7)	0.40 (10.0)	3.75 (19.2)	14.52 (70.8)
PPIX (pH 9)	0.43 (15.8)	3.61 (26.3)	13.39 (57.9)
PPIX (pH 11)	0.25 (21.7)	3.11 (21.7)	14.30 (56.6)

Values in parentheses indicate percentages.

all pH(s), except pH 2, r_∞ (limiting anisotropy) of ~0.1 are obtained which corresponds to rigid binding of PPIX to HSA along with hindered rotation of PPIX in HSA environment. If the temporal anisotropy curves were fitted using biexponential decay without a constant value of r_∞ (data not shown) a longer time constant of ~100 ns were obtained. Thus the r_∞ corresponds to a long rotational time constant (τ_{rot}) of ~100 ns which is the time constant of the global tumbling motion of the HSA molecule consistent with that obtained from SED relation (see above). Except at pH 2, a short rotational time constant of 0.03–0.04 ns is also observed which may be due to librational motion of PPIX at its binding site in HSA. Similar faster re-orientational motion of 15 ps or less time scale was observed, when a fluorescence probe ethidium bromide having rotational time constant of ~100 ps in water was intercalated in a rigid environment between the base pairs of genomic DNA [47]. At pH 2, the faster rotational time constant of 0.2 ns and $r_\infty = 0.02$ indicate that at this pH where domain-I expands and intra-domain structure disrupts [40], the porphyrin molecule becomes free to rotate at its binding site without actually leaving the site. In order to quantify the inter-domain separation between IB and IIA in various conformations of HSA, Förster's resonance energy transfer (FRET) technique is applied. Here, the non-radiative transfer of excited state energy from the intrinsic donor fluorophore Trp214 in subdomain-IIA to the acceptor molecule PPIX in subdomain-IB is considered (Scheme 1). Fig. 4a shows a significant spectral overlap of the Trp emission spectrum and PPIX-absorption spectrum at pH 7. Also, huge quenching of Trp fluorescence in the presence of PPIX is observed (Fig. 4b). Fig. 4c shows the fluorescent decay transients of N-form HSA both in the absence and presence of PPIX. The fluorescence lifetimes of Trp214 emission for various conformations of HSA are tabulated in Table 3. As evidenced from Fig. 4c and Table 3, much faster decay of tryptophan fluorescence is observed in presence of PPIX indicative of significant energy transfer. The calculated values of overlap integral ($J(\lambda)$), energy transfer efficiency (E), Förster's radius (R_0) and donor–acceptor (DA) separation (R) are tabulated in Table 4 for different conformations of HSA. The DA separation between Trp214 and PPIX for N-form HSA is 25.4 Å. This distance is in very good agreement with the distance (26.6 Å) between centers of Trp214 and Hem605 obtained from crystal structure of HSA–PPIX complex [5] (Scheme 1). In the alkaline pH range the DA separation decreases for B-form while that for A-form is comparatively higher than that for N-form. In acidic pH range for F-form HSA the DA separation is similar as that for N-form but for E-form HSA there is a large increase in DA distance from 25.4 Å to 33.9 Å. This is consistent with the increase in inter-domain separation and disruption of domain-I, thus showing a significant loss in native structure in N–E transition [40]. Such a high structural loss is not observed in case of N–A transition in alkaline pH range. Earlier an attempt has been made to explore the inter-domain (II-I) distance of HSA by covalent labeling of Cys34 and steady-state fluorescence quenching of Trp214 at various pH of the host solution [48]. While the trend of the inter-domain separation qualitatively matches with our observation, the exact inter-domain separation of 35 Å at pH 7.0 is *not* consistent with our value of 25.4 Å. The reason behind the difference between our data and

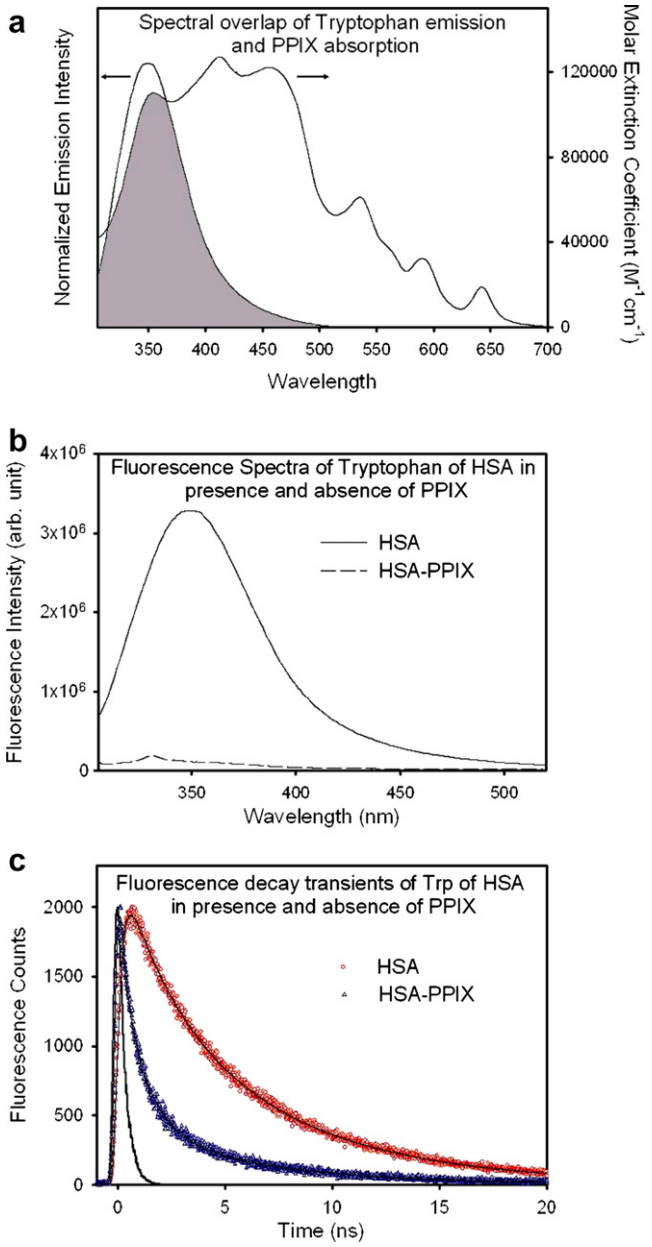

Fig. 4. (a) Spectral overlap of Fluorescence spectrum of Trp214 and absorption spectrum of PPIX bound to HSA at pH 7, (b) Fluorescence spectra (excitation = 297 nm) and (c) Fluorescence decay transients of Trp214 (excitation = 299 nm, emission = 360 nm) in presence and absence of PPIX bound to HSA.

the previous experimental result [48] is due to the fact that in the earlier study the donor and acceptor reside simultaneously in domain-IA and -IIA, respectively, and not IB and IIA, which is the case in the present study. The X-ray crystal structure of methemalbumin indicates that there is definite geometric arrangement of hem605 and Trp214, thus κ^2 cannot be taken to be 0.67. In this case we have calculated the κ^2 value to be 0.9853 using Eq. (7) from the crystal structure of methemalbumin [5] and used the same for calculation of DA separation. The assumption of κ^2 value of 0.67 leads to DA separation of

Table 3
Fluorescence lifetimes (τ) of Trp214 residue of HSA both in absence (denoted as HSA) and presence of protoporphyrin IX (denoted as HSA–PPIX)

Samples	τ_1 (ns)	τ_2 (ns)	τ_3 (ns)
HSA (pH 2)	0.23 (31.4)	1.97 (37.2)	5.65 (31.4)
HSA–PPIX (pH 2)	0.09 (72.5)	1.88 (15.0)	5.60 (12.5)
HSA (pH 4)	0.25 (34.3)	2.18 (31.4)	5.79 (34.3)
HSA–PPIX (pH 4)	0.04 (95.0)	1.67 (2.5)	5.63 (2.5)
HSA (pH 7)	0.28 (28.1)	2.73 (28.1)	7.01 (43.8)
HSA–PPIX (pH 7)	0.06 (90.8)	1.22 (6.6)	5.83 (2.6)
HSA (pH 9)	0.20 (36.1)	2.32 (25.0)	6.65 (38.9)
HSA–PPIX (pH 9)	0.08 (88.9)	1.04 (7.4)	4.01 (3.7)
HSA (pH 11)	0.14 (61.8)	1.90 (18.2)	5.71 (20.0)
HSA–PPIX (pH 11)	0.09 (89.7)	1.32 (6.9)	5.33 (3.4)

Values in parentheses indicate percentages.

23.8 Å at pH 7.0, which is 2.8 Å less than the value obtained from the crystal structure.

In order to quantify the inter-domain separation between domain-IB and IIIA by using FRET technique, the PPIX labeled HSA molecule is further labeled with an extrinsic dye TNS which like other hydrophobic dye (triiodobenzoic acid, TIB) expectedly occupies the hydrophobic cavity in the subdomain-IIIA of HSA [3]. Upon complexation with HSA, TNS shows a 61 nm blue shift in the steady-state emission spectrum compared to that in bulk water (485 nm). Fig. 5a shows the fluorescence transients of TNS bound to three different conformers of HSA. At all pH(s), three time constants of the order ~0.3 ns, ~4 ns and ~11 ns are observed (see Table 5). The multiple fluorescence lifetimes of TNS in HSA could be reflective of the probe in two different binding sites [49] of the protein. In such case the distance between TNS and PPIX as revealed from FRET experiment would be an average donor–acceptor distance in the protein. The shortest time constant corresponds to the lifetime of those TNS molecules which are loosely (electrostatically) bound at the surface of HSA [49], while ~4 ns and ~11 ns components are the state lifetime of locally excited (LE) state of TNS [50] bound to HSA in the hydrophobic cavity. Fig. 5b–d shows the temporal fluorescence anisotropy decay curve of TNS bound to various conformers of HSA. Two rotational time constants (φ) for TNS bound to HSA at all pH(s) are observed (Table 6). The shorter time constant of ~0.1−1 ns indicates the local reorientational motion of the TNS at its binding site. The relatively longer time constants of ~12−21 ns are significantly faster than the global tumbling time constants of the various pH-induced conformers of HSA as revealed from DLS experiments (see above) and hence we qualitatively assign the time constants (~12−21 ns) to the tumbling of the TNS-binding domain. A limiting anisotropy (r_∞) of ~0.06−0.1 for different pH-induced conformers of HSA indicative of higher degree of restriction on the rotation of the bound dyes is observed. It also indicates the fact that HSA has higher overall rotational time constant of ~100 ns (consistent with the rotational time constant obtained using SED

Table 4
Amplitude-weighted lifetime of HSA (τ_D) and HSA–PPIX complex (τ_{DA}), and calculated values of energy transfer efficiency (E), overlap integral ($J(\lambda)$), Forster's radius (R_0) and donor–acceptor distance (R) obtained from FRET between Trp214 (domain-IIA) and PPIX (domain-IB) in HSA at different pH(s)

Samples	$\langle\tau_D\rangle$ (ns)	$\langle\tau_{DA}\rangle$ (ns)	E	$J(\lambda)$ (M^{-1} cm^{-1} nm^4)	R_0 (Å)	R (Å)
pH 2	2.58	1.05	0.59	1.92×10^{15}	36.1	33.9
pH 4	2.75	0.22	0.92	2.47×10^{15}	37.5	25.0
pH 7	3.91	0.29	0.93	1.96×10^{15}	38.7	25.4
pH 9	3.24	0.30	0.91	1.82×10^{15}	34.8	23.8
pH 11	1.57	0.35	0.78	1.86×10^{15}	33.0	26.8

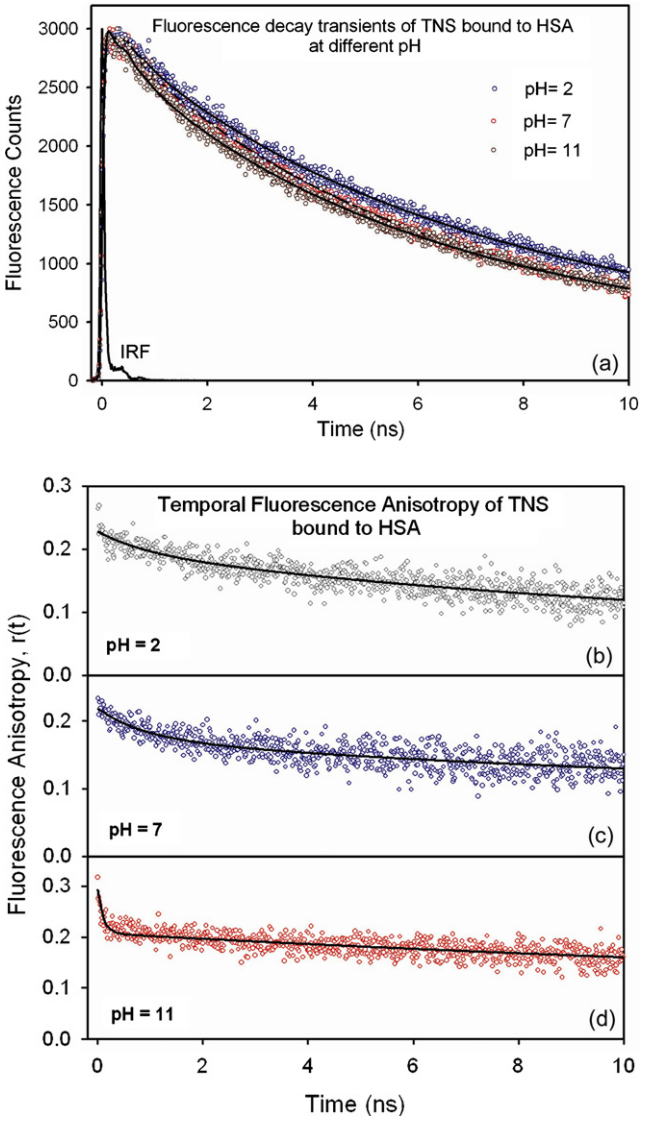

Fig. 5. (a) Fluorescence decay transients and temporal fluorescence anisotropy decay (excitation = 375 nm, emission = 440 nm) of TNS bound to HSA at pH(s): (b) 2, (c) 7 and (d) 11.

relation), which were obtained when the temporal anisotropy curve of different TNS-bound pH-induced conformers of HSA were fitted with triexponential decay function (data not shown). However, the longer rotational time constant of ~100 ns obtained through temporal anisotropy decay

Table 5
Fluorescence lifetimes of TNS bound to HSA both in absence (denoted as TNS) and presence of protoporphyrin IX (denoted as TNS–PPIX)

Samples	τ_1 (ns)	τ_2 (ns)	τ_3 (ns)	τ_4 (ns)
pH 2, TNS	0.29 (19.6)	3.70 (23.8)	11.14 (56.6)	–
pH 2, TNS–PPIX	0.21 (24.3)	3.55 (23.7)	11.14 (52.0)	–
pH 4, TNS	0.28 (23.6)	4.01 (30.6)	11.52 (45.8)	–
pH 4, TNS–PPIX	0.26 (35.1)	3.50 (27.3)	11.43 (37.6)	–
pH 7, TNS	0.23 (22.8)	4.39 (37.6)	11.09 (39.6)	–
pH 7, TNS–PPIX	0.20 (56.9)	2.69 (21.6)	10.42 (21.5)	–
pH 9, TNS	0.21 (25.7)	4.10 (34.2)	11.10 (40.1)	–
pH 9, TNS–PPIX	0.05 (77.5)	0.58 (13.1)	3.32 (6.0)	11.73 (3.4)
pH 11, TNS	0.27 (26.4)	3.56 (29.1)	11.30 (44.6)	–
pH 11, TNS–PPIX	0.05 (74.0)	0.66 (13.6)	4.19 (8.3)	15.31 (4.1)

Values in parentheses indicate percentages.

Table 6
Rotational time constants (φ), initial anisotropy (r_0), limiting anisotropy (r_∞) and semicone angle (θ_w) of TNS bound to HSA at different pH(s)

Samples	φ_1 (ns)	φ_2 (ns)	r_0	r_∞	θ_w
pH 2	0.96 (0.18)	12.0 (0.82)	0.23	0.06	20°
pH 4	0.58 (0.14)	21.6 (0.86)	0.21	0.07	18°
pH 7	0.85 (0.36)	13.6 (0.64)	0.23	0.09	31°
pH 9	0.80 (0.27)	20.0 (0.73)	0.23	0.08	26°
pH 11	0.10 (0.39)	14.8 (0.61)	0.28	0.10	32°

β_i—values are given in parentheses.

is not reliable in our 20 ns experimental time window. Thus, the fluorescence anisotropy data indicates that at all pH TNS remains bound to HSA. We have also calculated the semicone angle (θ_w) (see Table 6) exhibited by the wobbling TNS molecules bound to different pH-induced conformers of HSA using Eq. (6).

Fig. 6a shows a significant spectral overlap of the donor TNS bound to HSA (domain-IIIA) and acceptor PPIX (domain-IB) indicative of significant non-radiative transfer of excited state energy from TNS to PPIX (Fig. 6b). It should be noted that the emission peak and nature of temporal fluorescence anisotropy of TNS in HSA in presence and absence of PPIX are same. This observation is consistent with the fact that TNS is not displaced by the incorporation of PPIX in HSA. The fluorescence decay transients for TNS bound to HSA at pH 7 both in absence and presence of acceptor PPIX are shown in Fig. 6c. The calculated

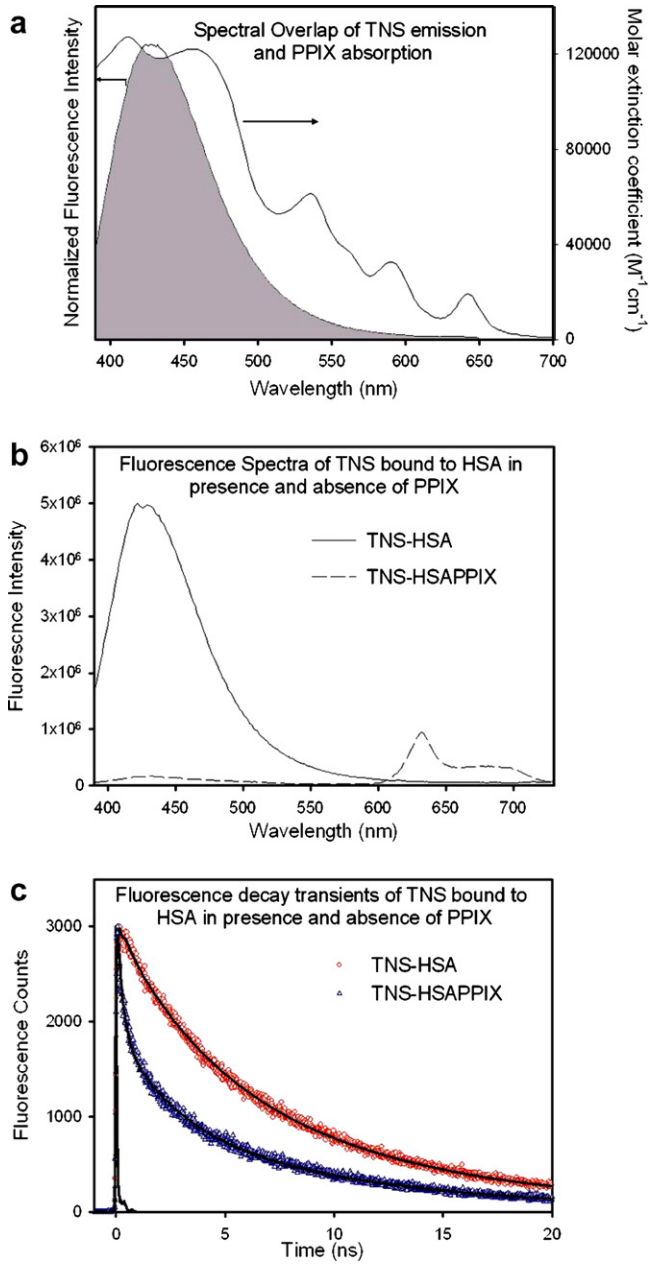

Fig. 6. (a) Spectral overlap of fluorescence spectrum of TNS bound to HSA (excitation = 375 nm) and absorption spectrum of PPIX bound to HSA at pH 7, (b) Fluorescence spectra (excitation = 375 nm) and (c) Fluorescence decay transients (excitation = 375 nm, emission = 440 nm) of TNS bound to HSA in presence and absence of PPIX.

values of overlap integral, energy transfer efficiency, Förster's radius and donor–acceptor (DA) separation are tabulated in Table 7 for different conformations of HSA. In this case due to the unavailability of the crystal structure of HSA with bound TNS the exact orientation of TNS and PPIX is not known. Under this circumstance κ^2 value is taken to be 0.67 [37]. From Table 7, it is found that DA separation between PPIX and TNS is 43.3 Å in N-form HSA. This distance further confirms the location of TNS to be in the domain-IIIA of HSA as revealed from inter-domain separation in X-ray crystallographic studies [5]. In acid pH range during N–F transition the DA separation changes to 54.7 Å and then to 74.2 Å when pH is reduced to pH 2. This is consistent with two-step expansion during N–E transition where first a structural loosening at the C-terminal end is observed during N–F transformation while for F–E transition further loss in tertiary structure along with secondary structural loss in domain-I of HSA are observed [40]. This fact is also supported by our DLS study. In alkaline pH range decrease in DA separation is observed (Table 7) which indicates that in alkaline pH range i.e. in N–B transition the structural rearrangement brings domain-IB and IIIA closer to each other. This is, however, not reflected through the contraction of hydrodynamic diameter in DLS study. It is worthy to mention that in the earlier study [51] the FRET using steady-state spectroscopy reveals the distance between covalently labeled Cys34 (domain-I) and Tyr411 (domain-III) to be 25.2 Å which differs from our observation of the I–III inter-domain distance of 43.3 Å and that from the X-ray crystallographic data [5] of 42.1 Å. This discrepancy in the previous literature [51] may arise due to the incorrect assumption of κ^2 value and/or erroneous determination of fluorescence quantum yield of the donor and the overlap integral of donor emission and acceptor absorption. It is to be noted that upon simultaneous incorporation both restricted and segmental motion into temporal anisotropy of the bound dye along with the effect of energy transfer brings complicacy in the interpretation of the anisotropy data which needs further refinement of the data analysis as depicted in the literature [52,53]. However, in this report our focus is to show the change in distance of different pH-induced conformers of HSA and not the effect of FRET on anisotropy.

Table 7
Amplitude-weighted lifetime of HSA–TNS (τ_D) and HSA–TNS–PPIX complexes (τ_{DA}), and calculated values of energy transfer efficiency (E), overlap integral ($J(\lambda)$), Forster's radius (R_0) and donor–acceptor distance (R) obtained from FRET between TNS bound to HSA (domain-IIIA) and PPIX (domain-IB) in HSA at different pH(s)

Samples	$\langle\tau_D\rangle$ (ns)	$\langle\tau_{DA}\rangle$ (ns)	E	$J(\lambda)$ (M^{-1} cm^{-1} nm^4)	R_0 (Å)	R (Å)
pH 2	7.24	6.68	0.08	5.36×10^{15}	49.0	74.2
pH 4	6.57	5.35	0.19	5.38×10^{15}	42.8	54.7
pH 7	6.1	2.94	0.52	4.46×10^{15}	43.9	43.3
pH 9	5.91	0.71	0.88	3.41×10^{15}	36.3	26.0
pH 11	6.14	1.1	0.82	2.86×10^{15}	34.7	26.9

4. Conclusion

In this study we have explored the ligand binding interaction of a very important transporter protein, human serum albumin in its different pH-induced folded states using picosecond-resolved polarization gated spectroscopy and Förster's resonance energy transfer technique. It is a multi-domain protein and adopts various conformations at different pH, a property that is very important for delivery of different kinds of drugs/ligands to their target cells. Two instances of energy transfer are considered – (a) between intrinsic fluorophore Trp214 and PPIX and (b) between an extrinsic probe TNS and PPIX. A good correlation of DA distances between the crystal structure of PPIX bound HSA [5] and our study is observed. The DA distances between PPIX and TNS bound to HSA at normal pH direct towards the probable location of TNS to be in domain-IIIA. Also, the study indicated significant structural perturbation of HSA at acidic pH, which is in consistence with our CD and DLS data. At alkaline pH, not much change in tertiary structure is observed. The time resolved fluorescence anisotropic studies reveal that at all pH TNS and PPIX remain bound to HSA. Thus, PPIX a non-covalent binder is proven to be a very efficient acceptor in reporting the inter-domain distances of different conformers of HSA at different pH.

Acknowledgements

A.K.S. thanks UGC for fellowship. We thank DST for financial Grant (SR/FTP/PS-05/2004).

References

[1] J.F. Foster, Some aspects of the structure and conformational properties of serum albumin, in: V.M. Rosenoer, M. Oratz, M.A. Rothschild (Eds.), Albumin, Structure, Function and Uses, Pergamon, Oxford, 1977.
[2] M. Dockal, D.C. Carter, F. Ruker, The three recombinant domains of human serum albumin, J. Biol. Chem. 274 (1999) 29303–29310.
[3] X.M. He, D.C. Carter, Atomic structure and chemistry of human serum albumin, Nature 358 (1992) 209–215.
[4] J. Ghuman, P.A. Zunszain, I. Petitpas, A.A. Bhattacharya, M. Otagiri, S. Curry, Structural basis of the drug-binding specificity of human serum albumin, J. Mol. Biol. 353 (2005) 38–52.
[5] M. Wardell, Z. Wang, J.X. Ho, J. Robert, F. Ruker, J. Ruble, D.C. Carter, The atomic structure of human methemalbumin at 1.9 Å, Biochem. Biophys. Res. Commun. 291 (2002) 813–819.
[6] A.M. Joussen, F.E. Kruse, M. Kaus, H.E. Volcker, Endogenous porphyrin for photodynamic therapy of cataracts in vitro, Opthalmologe 94 (1997) 428–435.
[7] J.M. Nauta, O.C. Speelman, H.L. van Leengoed, P.G. Nikkels, J.L. Roodenburg, W.M. Star, M.J. Witjes, A.J. Vermey, In vivo photodetection of chemically induced premalignancy lesions and squamous cell carcinoma of the rat palatal mucosa, Photochem. Photobiol. B: Biol. 39 (1997) 156–166.
[8] D. Kessel, Porphyrin-lipoprotein association as a factor in porphyrin localization, Cancer Lett. 33 (1986) 183–188.
[9] V. Jain, H. Goel, in: V. Jain (Ed.), Selected Topics in Photobiology, Indian Photobiological Society, New Delhi, 1992, pp. 130–147.
[10] N.C. Maiti, S. Mazumdar, H-aggregates of porphyrin–surfactant complexes: time-resolved fluorescence and other spectroscopic studies, J. Phys. Chem. B 102 (1998) 1528–1538.
[11] N.C. Maiti, M. Ravikanth, S. Mazumdar, N. Periasamy, Fluorescence dynamics of noncovalently linked porphyrin dimers and aggregates, J. Phys. Chem. 99 (1995) 17192–17197.
[12] S.B. Brown, M. Shillcock, Equilibrium and kinetic studies of the aggregation of porphyrins in aqueous solution, Biochem. J. 153 (1976) 279–285.
[13] R. Margalit, N. Shakla, S. Cohen, Fluorescence studies on the dimerization equilibrium of protoporphyrin IX and its haemato derivative, Biochem. J. 209 (1983) 547–552.
[14] S.M.B. Costa, M.M. Velazquez, N. Tamai, I. Yamazaki, Luminescence of porphyrins, J. Lumin. 48–49 (1991) 341–351.
[15] B. Cunderlikova, E.G. Bjorklund, E.O. Pettersen, J. Mohan, pH-Dependent spectral properties of HPIX, TPPS2a, mTHPP and mTHPC, Photochem. Photobiol. 74 (2001) 246–252.
[16] A.S.R. Koti, J. Taneja, N. Periasamy, Control of coherence length and aggregation size in the J-aggregate of porphyrin, Chem. Phys. Lett. 375 (2003) 171–176.
[17] N. Mataga, H. Chosrowjan, S. Taniguchi, Ultrafast charge transfer in excited electronic states and investigations into fundamental problems of exciplex chemistry: our early studies and recent developments, J. Photochem. Photobiol. C: Photochem. Reviews 6 (2005) 37–79.
[18] M.Y. Okamura, G. Feher, D.L. Nelson, Reaction centres, in: Govindjee (Ed.), Photosynthesis: energy conversion by plant and bacteria, Academic Press, New York, 1982, pp. 195–272.
[19] A.S. Davydov, Theory of Molecular Excitons, Plenum Press, New York, 1971.
[20] R. Margalit, M. Rotenberg, Thermodynamics of porphyrin dimerization in aqueous solutions, Biochem. J. 219 (1984) 445–450.
[21] P. Kubat, K. Lang, P. Anzenbacher Jr., Modulation of porphyrin binding to serum albumin by pH, Biochim. Biophys. Acta 1670 (2004) 40–48.
[22] S.M. Andrade, S.M.B. Costa, Spectroscopic Studies on the interaction of a water soluble porphyrin and two drug carrier proteins, Biophys. J. 82 (2002) 1607–1619.
[23] Y.-B. Yin, Y.-N. Wang, J.-B. Ma, Aggregation of two carboxylic derivatives of porphyrin and their affinity to bovine serum albumin, Spectrochim. Act A 64 (2006) 1032–1038.
[24] R. Galantai, I. Bardos-Nagy, K. Modos, J. Kardos, P. Zavodszky, J. Fidy, Serum albumin–lipid membrane interaction influencing the uptake of porphyrins, Arch. Biochem. Biophys. 373 (2000) 261–270.
[25] S. Cohen, R. Margalit, Binding of porphyrin to human serum albumin: structure–activity relationships, Biochem. J. 270 (1990) 325–330.
[26] J.-G. Liang, X.-P. Ai, Z.-K. He, H.-Y. Xie, D.-W. Pang, Synthesis and characterization of CdS/BSA nanocomposites, Mater. Lett. 59 (2005) 2778–2781.
[27] R. Sarkar, S. Shankara Narayanan, L.-O. Pa°lsson, F. Dias, A. Monkman, S.K. Pal, Direct conjugation of semiconductor nanocrystals to a globular protein to study protein-folding intermediates, J. Phys. Chem. B 111 (2007) 12294–12298.
[28] S. Shankara Narayanan, R. Sarkar, S.K. Pal, Structural and functional characterization of enzyme-quantum dot conjugates: covalent attachment of CdS nanocrystal to α-chymotrypsin, J. Phys. Chem. C 111 (2007) 11539–11543.
[29] J.A. Luetscher, Serum albumin. II. Identification of more than one albumin in horse and human serum by electrophoretic mobility in acid solution, J. Am. Chem. Soc. 61 (1939) 2888–2890.
[30] J.F. Foster, The Plasma Proteins, Academic Press, New York, 1960.
[31] W. Qiu, L. Zhang, O. Okobiah, Y. Yang, L. Wang, D. Zhong, A.H. Zewail, Ultrafast Solvation dynamics of human serum albumin: correlations with conformational transitions and site-selected recognition, J. Phys. Chem. B 110 (2006) 10540–10549.
[32] D.V. O'Connor, D. Philips, Time Correlated Single Photon Counting, Academic Press, London, 1984.

[33] J.R. Lakowicz, Principles of Fluorescence Spectroscopy, Kluwer Academic/Plenum, New York, 2006.
[34] A.K. Shaw, S.K. Pal, Fluorescence relaxation dynamics of acridine orange in nanosized micellar systems and DNA, J. Phys. Chem. B 111 (2007) 4189–4199.
[35] K. Kinosita Jr., S. Kawato, A. Ikegami, A theory of fluorescence polarization decay in membranes, Biophys. J. 20 (1977) 289–305.
[36] G. Lipari, A. Szabo, Effect of librational motion on fluorescence depolarization and nuclear magnetic resonance relaxation in macromolecules and membranes, Biophys. J. 30 (1980) 489–506.
[37] J.R. Lakowicz, Principles of Fluorescence Spectroscopy, Kluwer Academic/Plenum, New York, 1999.
[38] K. Das, B. Jain, H.S. Patel, Hydrogen bonding properties of coumarin 151, 500, and 35: the effect of substitution at the 7-amino position, J. Phys. Chem. A 110 (2006) 1698–1704.
[39] P. Debye, Polar Molecules, Dover, New York, 1929.
[40] M. Dockal, D.C. Carter, F. Ruker, Conformational transitions of the three recombinant domains of human serum albumin depending on pH, J. Biol. Chem. 275 (2000) 3042–3050.
[41] M.R. Eftink, C.A. Ghiron, Exposure of tryptophyl residues in proteins. Quantitative determination by fluorescence quenching studies, Biochemistry 15 (1976) 672–679.
[42] J.N. Phillips, Physico-chemical properties of porphyrins, in: M. Florkin, E. Stotz (Eds.), Comprehensive Biochemistry, Elsevier, Amsterdam, 1963, p. 34.
[43] R.C. Srivastava, V.D. Anand, W.R. Carper, A fluorescence study of hematoporphyrin, Appl. Spectrosc. 27 (1973) 444–449.
[44] U. Hofstra, R.B.M. Koehorst, T.J. Schaafsma, Excited-state properties of water-soluble porphyrin dimers, Chem. Phys. Lett. 130 (1986) 555–559.
[45] A.S.R. Koti, N. Periasamy, Self-assembly of template-directed J-aggregates of porphyrin, Chem. Mater. 15 (2003) 369–371.
[46] L. Brancaleona, S.W. Magennis, I.D.W. Samuelb, E. Namdasb, A. Lesara, H. Moseleya, Characterization of the photoproducts of protoporphyrin IX bound to human serum albumin and immunoglobulin G, Biophys. Chem. 109 (2004) 351–360.
[47] D.P. Millar, R.J. Robbins, A.H. Zewail, Direct observation of the torsional dynamics of DNA and RNA by picosecond spectroscopy, Proc. Natl. Acad. Sci. USA 77 (1980) 5593–5597.
[48] M. Suzukida, H.P. Le, F. Shahid, R.A. Mcpherson, E.R. Birnbaum, D.W. Darnall, Resonance energy transfer between cysteine-34 and tryptophan-214 in human serum albumin. Distance measurements as a function of pH, Biochemistry 22 (1983) 2415–2420.
[49] R. Wang, F.V. Bright, Detailed investigation of 2-(*p*-toluidinyl) naphthalene-6-sulfonate (TNS) binding to bovine serum albumin (BSA) by steady-state and time-resolved fluorescence spectroscopy, Appl. Spectrosc. 47 (1993) 792–799.
[50] D. Zhong, S.K. Pal, A.H. Zewail, Femtosecond studies of protein-DNA binding and dynamics: Histone I, Chem. Phys. Chem. 2 (2001) 219–227.
[51] N. Hagag, E.R. Birnbaum, D.W. Darnall, Resonance energy transfer between cysteine-34, tryptophan-214, and tyrosine-411 of human serum albumin, Biochemistry 22 (1983) 2420–2427.
[52] P. Wahl, J. Paoletti, J.-B. Le Pecq, Decay of fluorescence emission anisotropy of the ethidium bromide-DNA complex evidence for an internal motion in DNA, Proc. Natl. Acad. Sci. USA 65 (1970) 417–421.
[53] M.I. Ranasinghe, P. Murphy, Z. Lu, S.D. Huang, R.J. Twieg, T. Goodson III, Temperature dependence of excitation energy transport in a benzene branching molecular system, Chem. Phys. Lett. 383 (2004) 411–417.